Scientia Iranica B (2015) 22(6), 2229–2239

Sharif University of Technology
**Scientia Iranica**
*Transactions B: Mechanical Engineering*
www.scientiairanica.com

*Research Note*

# Design and simulation of a heating system for water purification structures in cold rural areas

**T. Zhang*, Y. Tan, J. Zhang and K. Yu**

*School of Municipal and Environmental Engineering, Harbin Institute of Technology, Harbin, 150090, China.*

Received 22 May 2014; received in revised form 3 June 2015; accepted 21 November 2015

**KEYWORDS**
Water purification structure;
Heating system;
Solar energy;
Straw boiler;
Numerical simulation.

**Abstract.** The settlement process and the biological treatment process of raw water purification can often not be completed efficiently under low ambient temperature in cold rural areas. Thus, a supplementary heating system is essential for water purification structures under these conditions. This paper proposes a novel hybrid heating system with a combination of solar heating and straw-boiler heating, in which the solar collectors and the straw boiler run in parallel as the heating source. The heat transfer model of the coagulation-sedimentation tank, the main heating position in a purification structure, has been established. Employing FLUENT software, the heat transfer conditions of different heating modes are simulated and analyzed to determine the optimal heating location. Then, the effect of the insulation thickness on heat loss is simulated, and, thus, the optimal thickness of the insulation layer is determined. Finally, for the novel heating system, the solar fraction and the duty ratio of the straw boiler in different months are calculated. Results show that the proposed heating system can perfectly meet the temperature demands of a water treatment plant in cold rural areas, and provide theoretical guidance and technical support for water purification structure heating in cold rural areas.



## 1. Introduction

Due to the extensive use of pesticides and fertilizers, the natural sources of rural drinking water have been severely polluted in China. Accordingly, conventional simple treatment processes are incapable of meeting water quality needs nowadays [1,2]. With the continuous development of China's rural water supply projects, water purification systems are being developed, from simple filtering devices to an integrated system that includes advanced equipment to accomplish coagulation, sedimentation and other advanced treatment processes [3].

In improved water treatment systems of rural China, the purification structure is the dominant department in which water treatment facilities are installed, and the water from a natural source is processed to meet the national standard of drinking water [4]. The structure mainly consists of two parts: the Coagulation-Sedimentation Tank (CST) and the Biologically Enhanced Filter Tank (BEFT) [5,6]. In the water treatment process, temperature is a key factor, which affects the speed and efficiency of purification processes in CST and BEFT. If the internal temperatures of the CST and BEFT cannot be maintained at required levels, the purification process may be adversely affected [7,8].

In the CST, by adding a particular species of coagulant, the particulate and flocculation matter in raw water gradually sinks under the force of gravity, and, thus, the solid matter separates from aqueous phases [9]. A hydrolysis reaction experiment, in which aluminum sulfate serves as the coagulant, has been

*. *Corresponding author. Tel.: +8613115605093*
*E-mail address: x418298537@163.com (T. Zhang)*

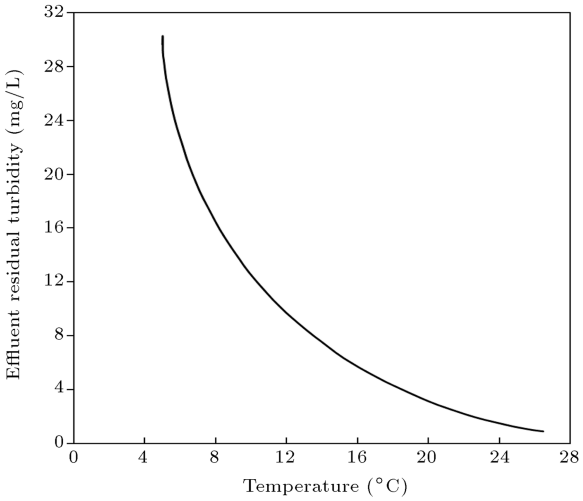


**Figure 1.** Effect of water temperature on effluent residual turbidity.

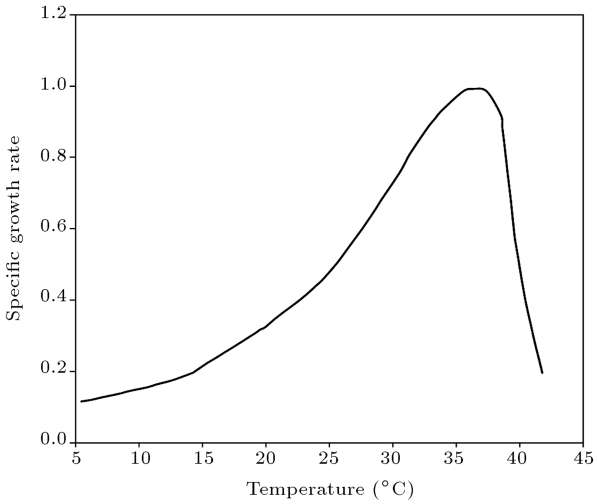


**Figure 2.** The change of microbial growth rate with temperature.

conducted to evaluate the influence of temperature on the settlement process [10]. Results show that under low temperature conditions, the floc forming speed is slow, and the flocculation particles are small, loose and with poor settleability. Even if the dose of the coagulant is increased, it is difficult to get a better coagulation effect. The reason is that the hydrolysis of inorganic coagulant is an endothermic process, thus, low temperature adds an extra degree of difficulty. With an input of 30 mg/L aluminum sulfate, when the temperature of the water being processed decreases by 10°C, hydrolysis rate declines by 50% to 75% (see Figure 1). When the water temperature is 5°C, the coagulant residue is almost 30 mg/L, thus, the hydrolysis rate is extremely slow, and the coagulation reaction almost stops. Therefore, to ensure an efficient coagulation process, it is necessary to maintain the water temperature above 10°C, and the higher the better [11].

The BEFT is a biological reactor in which the micro-biological degradation of pollutants is the main reaction inside. From the aspect of dynamics of cell growth (see Figure 2), the growth rate of the microorganism cells changes with temperature [12]. The higher the growth rate, the better the microbial activity is, the more sufficient the treatment process is, and the better the quality of the produced water is. When the temperature is below 10°C, microbial cell growth becomes very slow. When the temperature is below 5°C, the microbe activity is stagnant and microbes begin to die. When the water temperature is 15°C, microbial activity is about twice the activity at 5°C. As the temperature grows above 37°C, the microbial growth rate starts to decrease sharply. To maintain the micro-biological degradation at a high level, the water temperature in the BEFT should be kept between 15°C and 37°C; the higher the better. Additionally, the internal temperature of the BEFT should be stable, otherwise, the temperature fluctuations may do harm to the biological reactions. Thus, the temperature fluctuation can be limited below 3°C.

For the vast northern region of China, if the water purification structure is placed in outdoors without thermal insulation measures and supporting heating systems, the water treatment system will fail to operate effectively in winter. Actually, the extremely low outdoor temperatures in winter not only make the biological process inefficient, but also result in the frost-heave phenomenon in the water purification structure itself. Therefore, different types of thermal insulation measures and heating systems are employed for water purification systems in the towns of cold regions, such as heating systems supported by central heating networks or electrical heating [13]. However, for villages and small towns of northern rural areas, due to economic restrictions and other reasons, it is inapplicable to implement a heating system suitable for cities and big towns in rural purification structures. So, it makes a lot of sense to develop a proper heating system for rural water purification systems [14].

This paper proposes a novel hybrid heating system for rural water purification structures with a combination of solar heating and straw-boiler heating, in which the solar collectors and the straw boiler run in parallel as the heating source [15,16]. We further build the heat transfer model of the CST and the BEFT. By employing FLUENT software, the heat transfer conditions of different heating modes are simulated and analyzed. The most suitable heating location is then determined. Afterward, the effect of the insulation thickness on heat loss is simulated to obtain the optimal thickness of the insulation layer. Finally, for the novel heating system, the solar fraction and the duty ratio of the straw boiler in different months

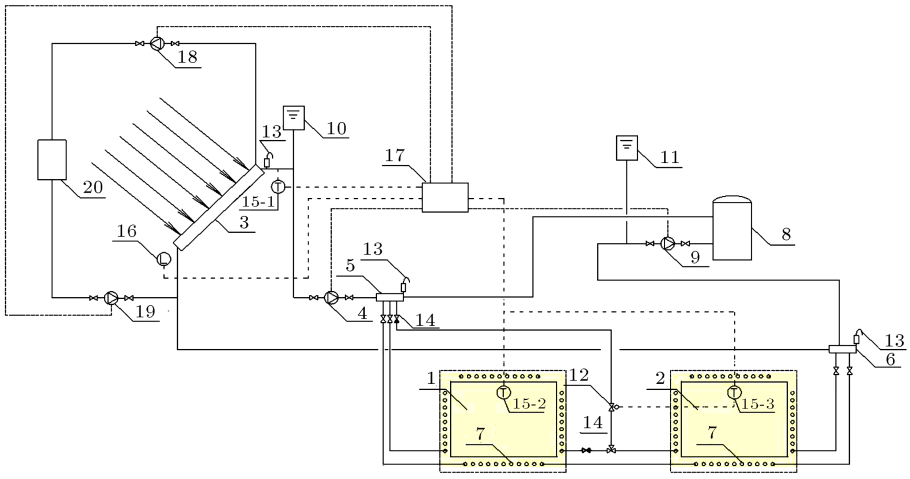


1. BEFT
2. CST
3. Solar collectors
4. Circulating pump
5. Water segregator
6. Water collector
7. Heating coils
8. Straw boiler
9. Circulating pump
10. Expansion tank
11. Water supply tank
12. Temperature control valve
13. Automatic exhaust valve
14. Check valve
15. Temperature sensor
16. Sun light intensity sensor
17. Controller
18. Drainage pump
19. Supply pump
20. Storage tank

**Figure 3.** System diagram of the combined heating system.

are calculated. Research results can provide theoretical guidance and technical support for water purification structure heating in cold rural areas.

## 2. Design and operational strategy of the novel heating system

Based on the actual situation of rural water treatment plants, a novel heating system that combines solar heating and straw boiler heating is proposed in this paper. The novel heating system mainly consists of the purification structure (the CST and the BEFT), circulation pumps, water separator, water collector, heating coils, temperature control devices, solar collectors, straw boiler, etc. (see Figure 3). All above facilities are constituted of two heating loops, the solar heating loop and the straw boiler heating loop. The solar collector and the straw boiler run in parallel as the heat source, which makes it easy to realize energy complementation and operation condition regulation. Since the low temperature raw water flows from the CST to the BEFT in the purification system in winter, the heating water is set to release high grade heat energy in the CST and then pass though the BEFT to consume low grade thermal energy, in consideration of energy cascade utilization. The heating load of the novel system can be divided into three parts: the heat loss of the CST, the heat loss of the BEFT and the heat absorption of raw water temperature rise. The heating coils can be located outside the top, the bottom, the sidewall of the CST, and the BEFT, or be placed in multiple locations.

In the solar and straw boiler combined heating system, the circulating power of the two heating loops is, respectively, provided by the circulating pumps 4 and 9. When solar radiation is abundant and the output of the solar collector is greater than the required heat of the water purification structure in the daytime, circulating pump 4 will be activated, while pump 9 will be closed. Hot water provided by the solar collectors will heat the CST and BEFT successively. If the heat provided by the solar collector fails to meet the heating demands of the structure, the controller will activate circulating pump 9, and the straw boiler will be put into use, together with the solar collectors, simultaneously. At nighttime or during continuous cloudy, rainy or snowy days, when solar radiation intensity is less than the preset minimum value, the straw boiler heating will be the operating loop, while the solar heating collector stops running. Accordingly, pump 9 will be activated and circulating pump 4 will be closed, and the hot water will be provided only by the straw boiler [4].

The controller (17) collects and analyzes the temperatures of the CST, the BEFT and the outlet temperature of the solar collector, and controls the system by adjusting the pumps located in different parts of the system. Other temperature control devices are employed for the BEFT to keep its temperature stable. Pumps 18 and 19, and storage tank 20 are installed to prevent freezing for the solar heating system. When the solar radiation intensity falls below the preset minimum value, pump 5 is stopped, while pumps 9, 18 and 19 are opened simultaneously to activate the straw boiler loop and to empty the solar loop. After that, pumps 18 and 19 are closed till the next time, when the intensity grows above the preset value, and are then opened to fill the solar collectors. The heating coils are located against the outer surface (including the sidewall, the top, and the bottom) of the

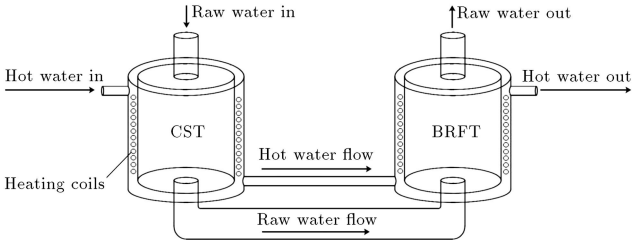


**Figure 4.** The water flows of the CST and BEFT.

CST and the BEFT. Extra insulation layers are added outside the heating coils. Different locations of the heating coils can realize different heating effectiveness. The influence of heating coil location will be discussed later in the paper.

In the actual operation mode of a water purification plant, the raw water flows through the CST and the BEFT, sequentially, to process an integrated treatment, as illustrated in Figure 4. In operation, the internal temperature has to be maintained above 10°C for both CST and BEFT. But, the heating load of the CST is much bigger than that of the BEFT, because low temperature raw water has to be heated to a proper level in the CST. In the proposed heating system, the produced hot water firstly heats the CST and secondly heats the BEFT, by which a better heating capacity is provided for heating the low temperature raw water, as well as offsetting the heat loss in the CST, while a lower capacity is generated only for offsetting the heat loss in the BEFT. The heating coils, in which the hot water circulates, are tightly wound around the outer surface of the purification structure. The order of the hot water and the location of the heating coils ensure a proper heating capacity for the purification structure. In the novel system, the raw water heating is processed in the CST, thus, the heating load of the heat loss and water heating in the CST occupies the major part. Consequently, the heat transfer of the CST is the dominant point in the following research.

Actually, the relationships among heat transfer in the CST, heat transfer in the BEFT, and hot and cold water flow are complex and coupled. It is difficult and unnecessary to find a global solution for the whole system. Besides, the main concern of this paper is to evaluate the heating effectiveness and influencing factors of the proposed system. Thus, the research centers of this paper focus on the heat transfer and flow characteristics of the CST.

## 3. Mathematical model and its solving conditions

According to our survey, the total water supply volume, which provides a design basis for the CST and BEFT, is 210 $m^3/d$. Thus, the design dimensions of the CST are 1.85 m and 4.05 m (diameter and height),

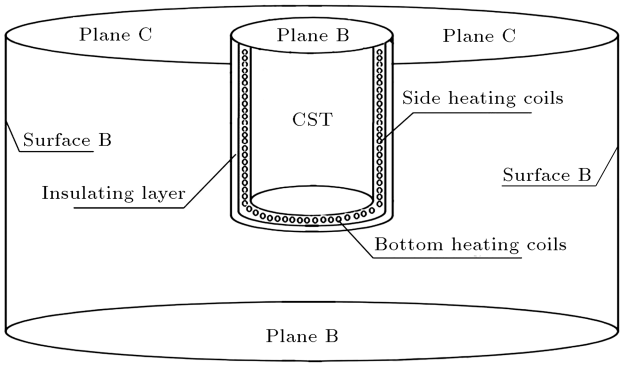


**Figure 5.** The mathematical model of the CST in the sidewall heating mode.

and 1.87 m and 3.85 m for the BEFT. Since heat transfer in the CST in the research is emphasised, for simplification, this paper employs a virtual cylinder, 2 m in diameter and 4 m in height, to represent the actual CST. The calculation involves heat exchange between the structures and the surrounding soil, so, the computational area is determined to be a cylinder soil area, 20 m in diameter and 20 m in height, since the soil temperature 18.5 m below ground level stays stable the whole year in Harbin city. Different types of heating mode can be applied for the CST and the BEFT, including the top heating mode, the sidewall heating mode and the bottom heating mode. Figure 5 illustrates the simulation model of the sidewall heating mode.

In the model, plane A is the interface between the model's bottom and surrounding soil, surface B represents the interface of the model's side boundary and soil, plane C is the interface between the model's upper surface and outdoor air, and plane D is the interface of the structure's upper surface and the air. The model can be used to simulate temperature distributions in typical operations or under different influences, for instance, under different heating modes or with insulation layers of different thicknesses.

To simplify to computation, the following assumptions are made:

1. The thermophysical property of the heat transfer fluid is constant with time and temperature;
2. The heat effect of the hydrolysis reaction is neglected;
3. The heating effectiveness of the heating coils is equivalent to surface heat sources with constant temperature;
4. The heat transfer process is treated as steady-state; the soil temperature changes with the depth but not with time;
5. The thermophysical property of soil is constant. The heat exchange between air and the soil surface

is surface heat convection; and the heat transfers between soil and the structure are only by means of heat conduction;

6. The layering phenomenon in the structure is neglected; the flow of water is neglected when modeling the temperature field.

According to the above assumptions, the problem in this paper is a steady-state heat transfer in cylindrical coordinates without an internal heat source. The mathematical model is:

$$\frac{1}{r}\frac{\partial}{\partial r}\left(\lambda r\frac{\partial t(r,\theta,z,\tau)}{\partial r}\right)+\frac{1}{r^2}\frac{\partial}{\partial \phi}\left(\lambda\frac{\partial t(r,\theta,z,\tau)}{\partial \phi}\right)=-\frac{\partial}{\partial z}\left(\lambda\frac{\partial t(r,\theta,z,\tau)}{\partial z}\right), \quad (1)$$

where $r$ is the distance between the concerned point and the axis (m); $z$ is the depth of the concern point (m); $\lambda$ is the thermal conductivity of the soil medium in the model (W/m.K).

### 3.1. The initial conditions

Since the water purification structure is placed underground, the initial soil temperatures can be obtained from the following formula:

$$\theta(z,\tau)=a_w.\exp\left(-z\sqrt{\frac{\pi}{aT}}\right)\cos\left(\frac{2\pi}{T}\tau-z\sqrt{\frac{\pi}{aT}}\right), \quad (2)$$

where $\theta(z,\tau)$ is the excess soil temperature at depth $z$ at moment $\tau$ (°C); $a_w$ is the amplitude of periodical temperature changes (K). The value for the Harbin area is 287.6 K; $a$ is soil thermal diffusivity ($m^2/s$); and $z$ is the depth (m).

### 3.2. The boundary conditions

Boundary conditions should be given at different parts of the structure, including the top, the sidewall, the bottom of the soil and the top of the structure:

1. The bottom of the soil (plane A): According to meteorological data, at a certain depth, soil temperature does not change with outside temperature. The boundary condition at plane A meets the first category of boundary condition. The soil temperature at a depth of 20 m from the ground surface is 7.2°C.

$$t|_{z=-20}=t_w=7.2^\circ\text{C}. \quad (3)$$

2. The side surface of the model (surface B): Ignoring the anisotropic of the soil's thermal conductivity, when the soil is far enough away from the water purification structure system, the soil temperature distribution is assumed to be free from the influence of the water treatment system. Therefore, in the model, the sidewall meets the second boundary condition.

$$q_w=\left.\frac{\partial t(\tau,r,z,\theta)}{\partial r}\right|_{r=10}=0. \quad (4)$$

3. The upper surface of the soil (plane C): Ignoring the radiation between the soil, the sky, and the surrounding air, the surface soil temperature is affected only by the natural convection between the soil surface and the air:

$$-\lambda(z)\left.\frac{\partial t(\tau,r,z,\theta)}{\partial z}\right|_{z=0}=h_w\left[t(\tau,r,z,\theta)-t_f\right], \quad (5)$$

where $h_w$ is the convective heat transfer coefficient between the ground surface and air (23 W/(m$^2$.K)); $t_f$ is the outdoor air temperature (°C).

4. The upper surface of the structure: Ignoring radiation between the top surface of the structure and the air, convection is considered to be the only heat transfer path at the top. The boundary condition is the third category:

$$-\lambda(z)\left.\frac{\partial t(\tau,r,z,\theta)}{\partial z}\right|_{z=0}=a_w[t(\tau,r,z,\theta)-t_f], \quad (6)$$

where $a_w$ is the convective heat transfer coefficient between the top and the air that, in this paper, is taken as 8.7 W/(m$^2$.K).

5. In the heating process of the coils, the wall thickness of the coils and the water temperature change in the coil are neglected. The water temperature in the coils is considered to be constant during the heating process. Thus, the interface of the structure's outer wall and the insulation layer, or the interface between the inner surface of the insulation layer and the heating coils, can be simplified as the first category of boundary condition:

$$t|_{r=1,-4.5\le z\le -0.5}=t_{\text{heat}}=T^\circ\text{C}, \quad (7)$$

where $t_{\text{heat}}$ is the temperature of the hot water in the coil; 30-60°C in this paper;

Detailed boundary conditions are listed in Table 1.

The simulation was processed directly for a single structure; the CST. The heating coils are located between the structure surface and the insulation layers. The parameters of relevant materials are listed in Table 2.

## 4. Results and discussions

### 4.1. The location of the heating coils

#### 4.1.1. The top heating mode

To determine the optimal location of the heating coils, a steady-state heat transfer condition of the CST is simulated to analyze and compare the temperature

**Table 1.** Boundary conditions in simulations.

| Boundary name | Material | Boundary type | Set value |
|---|---|---|---|
| Plane C | Soil | The second boundary condition | Convective heat transfer coefficient: 23 W/m$^2$.K<br>Temperature: 254 K |
| Plane A | Soil | The first boundary condition | Temperature: 280 K |
| Surface B | Soil | The third boundary condition | Heat flux intensity: 0 W/m$^2$ |
| Internal surface of CST | Galvanized steel | Coupling surface | — |
| Plane B | Glass wool | The second boundary condition | Convective heat transfer coefficient: 8.7 W/m$^2$.K<br>Temperature: 254 K |
| Insulation layer boundary | Glass wool | Coupling surface | — |
| Top heating coils | PE-X | The first boundary condition | Temperature: 333 K ∼ 303 K |
| Sidewall heating coils | PE-X | The first boundary condition | Temperature: 333 K ∼ 303 K |
| Bottom heating coils | PE-X | The first boundary condition | Temperature: 333 K ∼ 303 K |

**Table 2.** Thermophysical parameters of relevant materials.

| Name | | Density (kg/m$^3$) | Specific heat (W/m.K) | Thermal conductivity (J/kg.K) |
|---|---|---|---|---|
| Soil | Water content $\leq$ 30% | 2125 | 1800 | 1.89 |
| | Water content $\leq$ 40% | 1975 | 2120 | 2.44 |
| | Water content $>$ 40% | 1825 | 2430 | 3.02 |
| Air | Temperature $\leq$ 10°C | 1.28 | 1007 | 0.0251 |
| | Temperature $\leq$ 20°C | 1.25 | 1007 | 0.0251 |
| | Temperature $>$ 40°C | 1.22 | 1007 | 0.0251 |
| Water | | 980 | 4170 | 0.058 |
| Thermal insulation material (glass wool) | | 100 | 750 | 0.058 |

distributions in different heating modes (including top heating, bottom heating and sidewall heating). Using the established model, the hot water temperature is set to be 60°C, the initial internal water temperature of the structure is 15°C, and there is no insulation layer outside the structure.

The temperature field of top heating condition is presented in Figure 6. The temperature of the top area is affected seriously by the heating coils, as the heating coils are located outside the top of the structure. The average heat fluxes at the top, the side, and the bottom of the structure are 450.55 W/m$^2$, 3.94 W/m$^2$, and -0.043 W/m$^2$, respectively (the direction from internal to external is chosen as the plus direction). The temperature drops as the depth increases, but the distribution of the temperature field is far from uniform, with a decline of 333 K at the top to 273 K at the bottom. Thus, the top heating mode could not meet the temperature requirement of the CST.

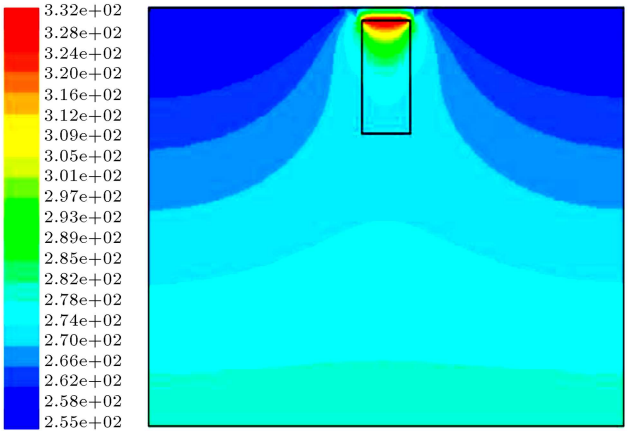


**Figure 6.** The temperature field of the top heating mode.

*4.1.2. The sidewall heating mode*

When the heat exchange coil is located against the side wall, the temperature distribution is more even (see Figure 7). The average heat flux density of the sidewall is 123.51 W/m$^2$ and the average heat flux densities at the top and bottom are 16.81 W/m$^2$ and 4.37 W/m$^2$, respectively. The temperature first increases and then decreases as the depth increases. When the hot water temperature is maintained at 60°C, the average internal temperature of the CST

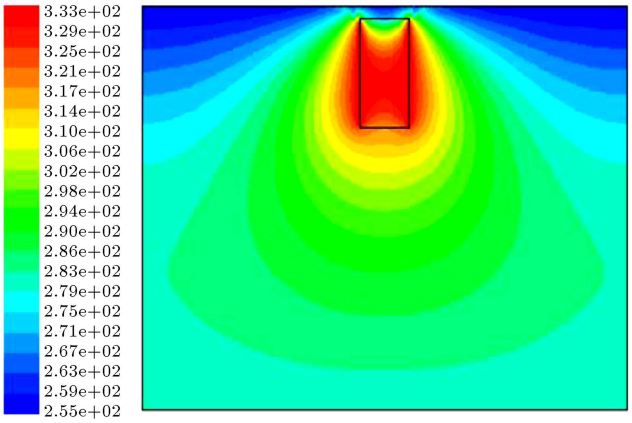


**Figure 7.** The temperature field of the sidewall heating mode.

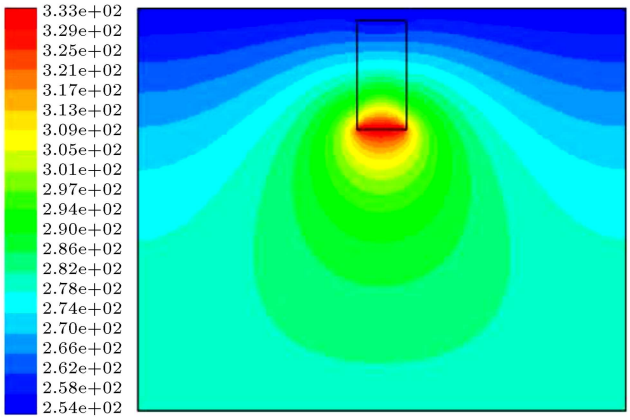


**Figure 8.** The temperature field of the bottom heating mode.

is about 40°C. Uniform temperature distribution and moderately warm temperatures under this mode ensure a high efficiency treatment process in the CST. So, the sidewall heating mode perfectly meets the heating demand of the CST.

*4.1.3. The bottom heating mode*

As presented in Figure 8, when the heat exchange coil is located at the bottom, the temperature distribution is uneven, and the top temperature is relatively low, which may result in water freezing at the top of the treatment structure. The temperature increases as the depth increases. The temperature varies rapidly from 258 K at the top to 333 K at the bottom. The average heat flux densities at the top, the sidewall and the bottom are 142.6 W/m$^2$, 1.8 W/m$^2$, and 4.37 W/m$^2$, respectively. So, the bottom heating is incapable of heating the CST effectively.

With the comparison of temperature fields under different heating modes, it is concluded that the sidewall heating mode has the best heating effectiveness for the CST. Additionally, in engineering practice, heating coils are mainly located against the sidewall, with insulation layers for structures which require necessary supporting heating systems, in consideration of the fact that there is a big heat loss at the sidewall in this heating mode. Thus, the optimal insulation thickness has to be determined in the sidewall heating mode. The top heating mode and bottom heating load could not work effectively alone. But, if necessary, a system with both top and bottom heating coils could be a more efficient way to meet relevant temperature requirements.

### *4.2. The thickness of the insulation layer*

To determine the optimal thickness of the sidewall heating mode, the heat transfer conditions of the CST under different thickness have been modeled. The initial and boundary parameters are consistent with those in the above section. But, the concerned models are modified by adding an insulation layer with different thicknesses outer the sidewall of the CST. Glass wool is chosen to be the insulation material, whose physical parameters are shown in Table 1. The insulation thickness varies from 5 cm to 35 cm, with an increasing step size of 5 cm. Figure 9 shows the simulation result by comparing the average heat flux intensity of the sidewall.

As can be seen from the figure, the sidewall heat flux decreases, that is, the heat preservation effect of the CST improves as the thickness of the insulation layer increases, but the decrease percentage declines. When the thickness is 5 cm, the net heat flux intensity is 7.85 W/m$^2$. The slope of the curve is big as the thickness grows from 5 cm to 20 cm, that is, the heat flux drops significantly when the thickness increases. However, the slope becomes much smaller as the thickness increases from 20 cm to 35 cm. Thus, the heat preservation effect is greatly enhanced when the thickness is smaller than 20 cm. But, when the thickness is bigger than 20 cm, increasing the thickness

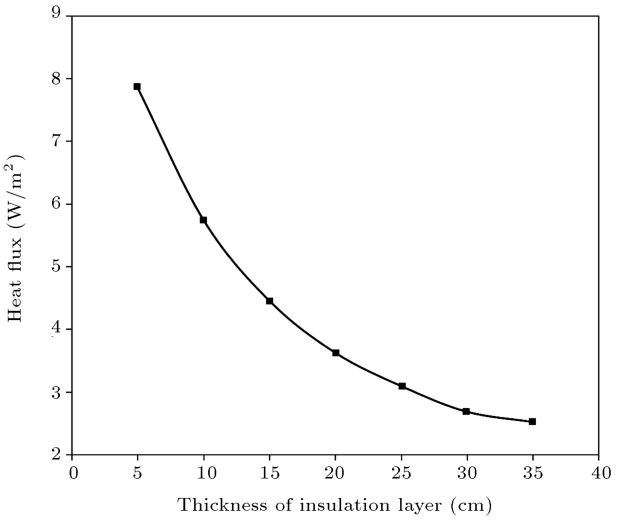


**Figure 9.** Sidewall heat flux under different insulation layer thickness.

has a weaker effect on the heat insulation of the CST. Consequently, 20 cm is the optimal insulation thickness in this system.

In the sidewall heating mode, the temperature field of the CST with a 20 cm insulation layer is illustrated in Figure 10. For comparison, the temperature field under the top and bottom combined heating mode is shown in Figure 11. In the sidewall heating mode, the average temperature is higher and the distribution is more uniform, while in the top and bottom combined heating mode, the average temperature is lower. According to the temperature requirements of the CST and the BEFT, the sidewall heating mode is more suitable for the treatment structure.

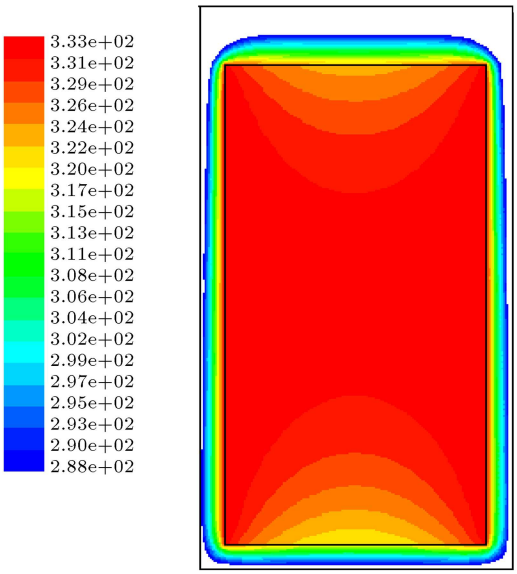


**Figure 10.** Temperature field under the sidewall heating with a 20 cm insulation layer.

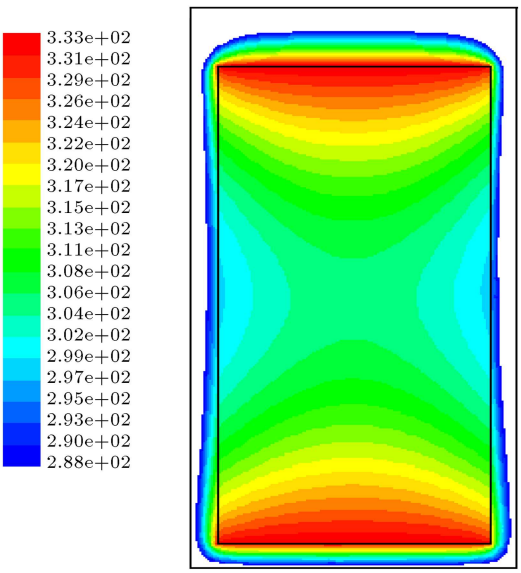


**Figure 11.** Temperature field under the top and bottom heating with a 20 cm insulation layer.

### *4.3. The influence of the hot water temperature*

In the previous sections, the hot water produced by the heating system was set to be 60°C in the simulation to evaluate the steady-state heat transfer condition of the CST, which gives a judgment to determine the heating mode and thickness of the insulation layer. However, in actual running condition, the hot water temperature changes with weather conditions, outdoor temperature and other factors. So, it is necessary to evaluate the influence of the hot water temperature on the internal temperature distribution. This section deals with this problem. Since the raw water temperature also impacts greatly on the internal temperature, a necessary improvement has to be made to the established model: Relevant inlet and outlet flow boundary conditions are added to the top and the bottom of the CST, respectively. The flow rate of the raw water is 0.25 kg/s and the inlet temperature is 2°C in Harbin City, in January. In the simulation, the hot water temperature is set with different values from 30°C to 60°C, in respect to the solar heating capacity. The average internal temperatures of the CST under different hot water temperatures are illustrated in Table 3.

As shown in Table 3, when the hot water in the heating coils is 30°C, the average temperature is 14.7°C, which meets the requirement of the treatment process in the CST. The heat release of the hot water is 661.58 W. As hot water temperature increases, both the average internal temperature and the heat release of the hot water increase. When the hot water temperature reached 60°C, the average temperature is 29.2°C. So, in the temperature region of 30°C to 60°C, the internal temperature of the CST can be promoted to a level at which the sedimentation can be processed at high efficiency. Thus, the proposed combined heating system has the ability to maintain the water treatment process in a purification structure at an efficient level.

**Table 3.** The average internal temperatures under different hot water temperatures.

| Hot water temperature (°C) | Average internal temperature of the CST (°C) | Heat release of the hot water (W) |
|---|---|---|
| 30 | 14.7 | 661.58 |
| 35 | 16.9 | 794.26 |
| 40 | 19.3 | 926.93 |
| 45 | 22.4 | 1059.59 |
| 50 | 24.1 | 1192.27 |
| 55 | 27.6 | 1324.92 |
| 60 | 29.2 | 1457.59 |

### 4.4. Duty ratios of solar collectors and straw boiler

#### 4.4.1. The heating loads and the solar heat gain

Based on the heat transfer conditions in different months, heating loads of the proposed heating system can be obtained, and then the duty ratios of the two energy resources can be calculated. For a purification system with a CST and a BEFT, the heating load of the proposed heating system consists of three parts: the heat loss of the CST, the heat loss of the BEFT and the heat energy required in heating low temperature raw water. If the operating temperatures of the CST and the BEFT are set to be the same, the heat losses of the two parts are also the same. Based on the previous simulation, the heat flux intensities at different parts of the CST, in different months, can be obtained, so that the heating load consumed by the CST and BEFT can be easily calculated, according to the heat transfer equations. Setting the operating temperature of the CST and the BEFT as 15°C, the results of the heat losses are presented in Table 4.

It can be observed that the heat losses from October to March are high, and from April to September are small. So, the heat loss decreases as the outdoor temperature increases. Furthermore, the raw water temperature increases as outdoor temperature increases, thus, the energy demand in raw water heating also decreases when the ambient temperature increases. Actually, in our calculation, the solar heating loop can provide all the heating energy from April to September. The later calculation focuses on the months with high heating loads, that is, from April to September.

The energy amount consumed in raw water heating can be calculated from the temperature difference between the unheated and heated raw water. The results are shown in Table 5.

To evaluate the duty ratios, the solar heat gain has to be provided. Necessary data are provided in Table 6.

#### 4.4.2. A case study on the duty ratios in different months

For a given solar thermal system, the solar fraction can be obtained from a non-dimensional formula [17]:

$$f = (102.9Y - 6.5X - 24.5Y^2 + 0.18X^2 + 2.15Y^3) \times 10^{-2}, \quad (8)$$

where $f$ is the solar fraction, and $X$ and $Y$ are dimensionless parameters which can be obtained as

**Table 4.** The heat release of the structure in different months.

| Month | Outdoor temperature (°C) | Heat release (W) | Month | Outdoor temperature (°C) | Heat release (W) |
|---|---|---|---|---|---|
| Jan. | -18.73 | 298.68 | Jul. | 22.85 | 64.46 |
| Feb. | -14.54 | 276.04 | Aug. | 20.95 | 74.73 |
| Mar. | -2.64 | 207.50 | Sep. | 14.71 | 105.61 |
| Apr. | 7.74 | 136.13 | Oct. | 5.16 | 187.91 |
| May | 14.2 | 110.13 | Nov. | -6.62 | 227.76 |
| Jun. | 20.02 | 75.26 | Dec. | -14.83 | 276.67 |

**Table 5.** Total heating loads of the heating system.

| Month | Oct. | Nov. | Dec. | Jan. | Feb. | Mar. |
|---|---|---|---|---|---|---|
| **Raw water temperature (°C)** | 3.8 | 3.5 | 3 | 2.7 | 2.4 | 2.2 |
| **Monthly heat loss (MJ)** | 16.2 | 19.7 | 23.9 | 25.8 | 23.8 | 17.9 |
| **Monthly load of raw water heating (MJ)** | 9878.4 | 10143 | 10584 | 10848 | 11113.2 | 11289.6 |
| **Total monthly load (MJ)** | 9895 | 10163 | 10608 | 10874 | 11137 | 11308 |

**Table 6.** Monthly heat gain of evacuated tube collectors in Harbin.

| Month | Oct. | Nov. | Dec. | Jan. | Feb. | Mar. |
|---|---|---|---|---|---|---|
| **Equivalent solar altitude** | 11.75 | 9.96 | 7.81 | 8.30 | 9.48 | 14.19 |
| **Average daily sunshine duration** | 10.59 | 9.28 | 8.58 | 8.91 | 10.09 | 11.69 |
| **Total power of collector ($W/m^2$)** | 364.89 | 273.04 | 206.67 | 208.82 | 275.41 | 471.91 |
| **Monthly heat gain (MJ)** | 431.243 | 273.652 | 197.892 | 206.826 | 280.112 | 615.656 |

follows:

$$X = \frac{891.67 \times A_c}{Q}, \tag{9}$$

$$Y = \frac{0.736 \times A_c \times H_g}{Q}, \tag{10}$$

where $Q$ is the monthly heating load of the heating system (MJ), as illustrated in Table 5; $A_c$ is the area of the solar collectors ($m^2$); and $H_g$ is the monthly heat gain of the solar collectors (MJ), as shown in Table 6.

For a rural solar system, the initial cost is the major constraint. In rural areas of China, 50,000 Yuan is the ceiling of a solar system. So the area of the solar collectors should be no more than 50 $m^2$. Assuming the area of the solar collectors in the proposed system is 50 $m^2$, the solar fractions in different months are shown in the curve of Figure 12.

In January, the solar fraction is 37.3%, so, the duty ratio of the straw boiler is 62.7%. Then, the heat provided by the straw boiler can be obtained by:

$$Q_g = Q(1 - f) = 6818 \text{ MJ}. \tag{11}$$

Then the duty ratio of the straw boiler in different months can be obtained, as illustrated in Table 7.

As for the proposed combined heating system with solar collectors and a straw boiler, the lowest solar fraction appears in January to be 37%, when the duty ratio of the straw boiler is the highest at 63%. From April to September, the solar heat gain would be sufficient for the heating load of the purification system. In other months, with the cooperation of the solar heating loop and the straw boiler heating loop, the system perfectly meets the heating demand. Thus, the combined heating system enjoys the advantages of strong reliability and high energy saving performance.

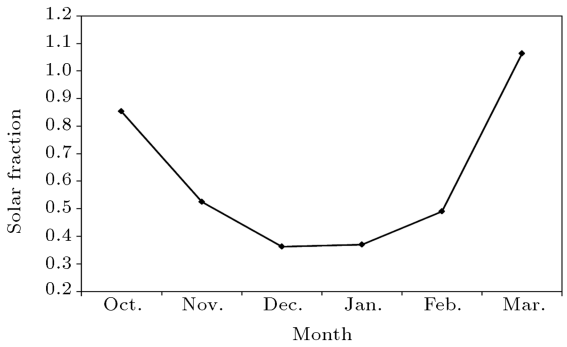


**Figure 12.** Solar fractions of the heating system in different months.

However, it should be noted that the combined heating system is specially designed for water purification structures in cold rural areas. All the above discussion is based on numerical simulation. The performance of the novel heating system under actual operating conditions and its applicability are still to be further investigated in our follow-up study.

## 5. Conclusion

For rural water purification structures in cold regions, a novel hybrid heating system, with the combination of solar heating and straw-boiler heating, is proposed in this paper. The heat transfer model of the CST has been established, solved under typical initial and boundary conditions.

Using the established model, the temperature fields of the CST under different heating modes are obtained. With the comparison of the temperature fields, it is concluded that the sidewall heating mode has the best heating effectiveness, as the sidewall heating provides a uniform temperature distribution and moderately internal temperatures for the CST.

The heat transfer conditions of the CST under different thicknesses have been modeled. The heat preservation effect of the CST improves as the thickness of the insulation layer increases. From a comprehensive consideration, 20 cm is the optimal insulation thickness in this system.

The produced hot water temperature has a big impact on the internal temperature of the CST. When the hot water temperature increases from 30°C to 60°C, the average internal temperature of the CST increases from 14.7°C to 29.2°C. In this temperature interval, the sedimentation can be processed at high efficiency.

The result of a case study shows that, for a combined heating system with a solar collector area of 50 $m^2$, the lowest solar fraction appears, in January, to be 37%, while the duty ratio of the straw boiler is the highest at 63%. In a whole year, with the collaboration of the solar collectors and the straw boiler, the combined heating system perfectly meets the heating demands of a purification structure.

## Acknowledgments

This research was financially supported by the National Twelfth Five-Year Technology Support Program: Integration and Demonstration of Drinking Water

**Table 7.** Duty ratios of the straw boiler in different months.

| **Month** | Oct. | Nov. | Dec. | Jan. | Feb. | Mar |
|---|---|---|---|---|---|---|
| **Heat load of the boiler (MJ)** | 1456.2 | 4801.6 | 6730.2 | 6818.4 | 5655.4 | -738.3 |
| **Duty ratio** | 15% | 47% | 63% | 63% | 51% | 0 |

Security Technology for Northeast Cold Rural Areas (2012BAJ25B10).

## References


1. Liu, W. "Characteristics and suggestions on small scare water treatment plants in rural area of China", *Science and Technology Innovation Herald*, **25**, pp. 105-107 (2010).
2. Yang, H., Wright, J.A. and Gundry, S.W. "Household water treatment in China", *The American Journal of Tropical Medicine and Hygiene*, **86**(3), p. 554 (2012).
3. Liu, X. and Zhou, S. "Zoning of rural water conservation in China: A case study at Ashihe river basin", *International Soil and Water Conservation Research*, **3**(2), pp. 130-140 (2015).
4. Zhang, Q. and Tao, Y. "Water supplying ratio and influencing factors analysis for centralized water plants in China rural area", *Journal of Environment and Health*, **29**(3), pp. 249-251 (2012).
5. Dana, M. and David, R.H. "Feasibility of water purification technology in rural areas of developing countries", *Journal of Environmental Management*, **88**(3), pp. 416-427 (2008).
6. Wood, D.M., Greenland, B.W., Acton, A.L. et al. "pH-tunable hydrogelators for water purification: Structural optimisation and evaluation", *Chemistry-A European Journal*, **18**(9), pp. 2692-2699 (2012).
7. Ifegwu, E., Anjaneyulu, K. "Sustainable rural development: solar/biomass hybrid renewable energy system", *Energy Procedia*, **57**, pp. 1492-1501 (2014).
8. Savinkina, E., Kuzmicheva, G. and Obolenskaya, L. "A novel titania-based photocatalyst for water purification", *Int. J. Energy Environ*, **6**(2), pp. 268-275 (2012).
9. Wang, S. "Exploration on influencing factors for coagulation effect", *Value Engineering*, **24**, pp. 109-110 (2010).
10. XU, Y., Zhao, H. "Analysis and solution of abnormal floc in sedimentation process", *Journal of Shijiazhuang Institute of Railway Technology*, **11**(4), pp. 60-63 (2012).
11. Yang, S. and Liu, Z. "The effect study of temperature on water purification performance of biological activated carbon reactor", *Journal of Northeast Dianli University*, **31**(5), pp. 151-154 (2011).
12. Copelli, S., Torretta, V., Raboni, M. et al. "Improving biotreatment efficiency of hot waste air streams: experimental upgrade of a full plant", *Chemical Engineering*, **1**, p. 30 (2012).
13. Gao, Y., *Widely Utilized Technologies in Water Supply Engineering*, Silicon Valley, **03**, p. 77 (2011).
14. Zhao, Ji. "Design and running modeling of water purification heating system in cold rural areas", Master's Thesis of Harbin Institute of Technology (2013).
15. Fan, H. and Chi, B. "A brief discussion on the solar collector and its applicability", *Journal of Qingdao Technological University*, **03**, pp. 118-121 (2009).
16. Tian, Y. and Zhao, L. "Technical-economic assessment on rural bio-energy utilization technologies in China", *Transactions of the Chinese Society of Agricultural Engineering*, **27**(1), pp. 1-5 (2011).
17. Liu, Ni and Yang, Y. "Assessment uncertainty of solar fraction measurement in a solar water supply system", *Journal of Yunnan Normal University*, **01**, pp. 21-24 (2013).


## Biographies

**Tiantian Zhang** was born in 1987, in Jingzhou, China. He received his BA and MS degrees from Harbin Institute of Technology, where he is currently a PhD degree student. His research interests focus on heat transfer, fluid mechanics, thermodynamics, solar energy, HVAC systems, gas supplying and renewable and sustainable energy technologies in buildings.

**Yufei Tan** was born in Harbin, China, in 1962. She is currently Professor in the School of Municipal and Environmental Engineering at the Harbin Institute of Technology, Harbin, China. Her research interests include heat transfer, fluid mechanics, thermodynamics, building energy efficiency, and heating ventilation and air conditioning system simulation and control.

**Jindong Zhang** was born in 1992, in Heilongjiang province, China. He received his BS and MS degrees from Harbin Institute of Technology, China, where he is currently pursuing his PhD degree. His research interests focus on solar energy, HVAC systems, gas supplying and renewable and sustainable energy technologies in buildings.

**Kecheng Yu** was born in 1991, in Niaoning province, China. He received his BS and MS degrees from Harbin Institute of Technology, China, where he is currently pursuing his PhD studies. His research interests focus on thermal insulation of underground pipelines, gas supplying and renewable and sustainable energy technologies in buildings.